D19

FLYWHEEL CONTAINMENT AND SAFETY CONSIDERATIONS

Anthony P. Coppa
General Electric Company
Space Systems Division
Box 8555, Philadelphia, Pennsylvania

INTRODUCTION

Considerable research and development work was directed during the past seven years to exploiting the large potential of flywheel energy storage systems [1-4]. These activities were spurred by the energy crisis and particular attention was focused on consumer passenger vehicle applications since these offered great promise of reducing petroleum fuel consumption on a world scale. In the United States, flywheel R&D programs were largely sponsored by the Department of Energy (DOE), through which the Lawrence Livermore National Laboratory (LLNL) played a principal role in directing and coordinating them. Under the Mechanical Energy Storage Technology (MEST) Project major advances were achieved in composite flywheel rotor design and fabrication technologies with a significant start in developing burst-containment design capability. A wide assortment of composite rotors featuring a variety of constructions and materials were produced during this effort. Table 1 lists some of these and identifies three generic rotor design categories, namely: rim, disk, and rim/disk hybrid types. In burst tests several rotors have demonstrated ultimate energy densities that approach the current DOE goal of 88 wh/kg for vehicular flywheels: The Garrett AiResearch multi-ring rim design obtained the best energy density, up to 79.4 wh/kg, and the General Electric ring/disk hybrid the best combination of weight and volumetric energy densities, i.e., 68.0 wh/kg and 115 kwh/m^3. Also, progress was made in durability testing: A modified Garrett rotor design was tested for 2586 spin cycles at energy density levels between 44.1 and 11 wh/kg. The DOE goal for operational energy density is 44-55 wh/kg. Two General Electric flywheels survived 10,000 cycles at lower energy density levels and went on later to yield high ultimate perfomance, up to 68 wh/kg. In the area of operational safety, composite rotor burst and containment processes for a variety of rotor constructions are now better understood as a result of detailed studies of spin test data [5,6]. This led to definition of flywheel housing prototype designs.

In addition to obtaining high performance, composite has been preferred to metallic rotor construction because of the relatively benign containment processes that are associated with rotor burst. In the early stages of the MEST Project, this awareness was based principally on observation of post-burst debris which showed that composite rotors fragment to a much higher degree than metallic rotors and indicated a much lower capability to inflict damage on a containment housing. Much experience, however, was available with metallic rotor bursts which showed very severe containment processes. Estimates of containment weight requirements for metallic rotors often indicated values several times greater than the rotor weight itself. Although metallic flywheel rotors that are designed to release relatively low damage-potential fragmentation upon failure have been produced [7], such approaches were not emphasized in major MEST project developments that were aimed at transportation vehicle applications. Instead, composite construction was favored because of the promise of higher energy density and intrinsically safer containment.

Early assessments of composite-rotor containment processes led some to underestimate the need for substantial containment devices. Tests performed [8] during the past three years, however, have shown that composite-rotor bursts can produce impressive amounts of damage in heavy containment structures, although the damage is still well below that produced by a comparable metallic rotor burst. An optimum system would most likely incorporate rotor and containment housing designs which offer the best combination of performance indices (energy, density, durability, and cost). A fail-safe rotor, viz, one that fails in a non-burst mode, would be preferable to one that might have a higher energy density but simultaneously a catastrophic burst mode of failure.

Containment therefore became a strong driver in the development of a satisfactory vehicular flywheel system, and toward the end of the DOE program efforts were underway to perform experiments involving composite rotor bursts within realistic vehicular-type housings. The only such experiment that was conducted before termination of the program demonstrated the severity of a high energy burst containment process, but circumstances did not provide an opportunity to explore the problem further and develop a design solution. It is judged that acceptable housing designs for ground transportation vehicles could have been developed, drawing upon the lessons learned from the first containment test and others that would have followed had the program continued. It is less certain, however, whether containment of a high energy burst is a feasible design requirement to satisfy in a space flywheel system, in view of a much lower tolerance for the associated weight penalty. The importance of minimizing the degree of containment requirements in space systems through use of essentially 'fail-safe' or 'limited failure' rotor designs has become increasingly recognized and is a subject that deserves early and adequate attention.

THE FLYWHEEL SAFETY ISSUE

The issue of flywheel safety is a subject of growing interest. With greater quantification of composite rotor burst effects and corresponding containment requirements, attention is being focussed on possible development of 'limited failure' even 'fail-safe' rotor designs. In response to this concern, two specific design approaches based on the General Electric hybrid flywheel which feature such failure properties were outlined [9]. The hybrid flywheel consists basically of a central disk and a filament-wound ring interference-fitted to the disk at its periphery. In recent designs, the ring has an inside to outside radius ratio (β) of .8. Spin tests performed on such rotors have demonstrated good ultimate energy densities ($\sim$68 wh/kg). The performance for this and other possible designs is shown in Figure 1, in which energy density is plotted against β for governing failure modes. Two sets of failure envelopes are shown, namely, short-time ultimate failure (solid curves) and 10^5 cyclic fatigue (dashed curves). For β = .8, the predicted failure modes are circumferential ring failure (CRF) and disk failure (DF) relative to ultimate and cyclic conditions respectively. Ultimate speed tests have in fact verified the CRF prediction. It would be desirable to avoid either type of failure in a space application because the associated containment weight penalty might be excessive. Designs based on values of $\beta < .77$, however, would be limited by the non-burst radial ring failure (RRF) mode for both conditions and at least theoretically would not require containment. Such a benefit would be gained at the expense of lower performance as evident in the Figure.

In order to establish an assured fail-safe composite rotor design practice along the lines illustrated in the previous example, material design properties will have to be established with greater reliability than presently available. Hence, materials specimen type as well as rotor spin tests, especially under cyclic conditions, should be initiated early in the process of developing composite rotors for space flywheel systems.

The above example is made to illustrate one of the trade-offs between performance and safety that can be systematically obtained through composite rotor design. Such an approach should be superior to one in which the rotor performance is merely

derated by a 'safety factor' in the attempt to obtain fail-safe operation because the latter practice would not intrinsically address a non-burst failure mode. Hence, an unresolved concern would exist about rotor safety for such a design in view of a possible, albeit improbable, burst failure event.

The second approach described in [9] illustrates the 'limited failure' rotor design technique. The example involves a radially thick filament-wound composite rotor ring which utilizes a flexible instead of a rigid matrix and its construction. For such a rotor, the limiting stress is confined to a relatively narrow radial zone at the outer periphery. Stresses inboard of this region are relatively low. Also, because of the large strain tolerance of the matrix, radial stresses would be held within acceptable bounds. Failure of such a rotor is expected to involve release of fragmentation only from the restricted region of maximum stress. The failure process would be self-arresting because of the lower interior stresses. Hence, containment would be required only for a relatively small portion of the rotor and the associated weight penalty would be acceptably low. Such an approach offers a high potential for energy storage performance in a space rotor. Spin tests, however, have not as yet been performed on such a design although rotors embodying flexible-matrix rings were produced under the DOE program.

By means of such design approaches as illustrated above, the issue of flywheel safety can be addressed systematically and ultimately resolved. The challenge will be to develop 'fail-safe' and/or 'limited-failure' rotor designs whose energy storage performance is not unduly compromised. Obviously, considerable testing will be required to demonstrate design reliability.

At least for the 'limited-failure' design approach, containment will have to be provided. Relative to the 'fail-safe' rotor approach, it remains to be seen whether in fact containment can be totally dispensed with. Design definition of containment requirements relative to the proposed rotor developments will be an important factor in determining the course of these developments. Hence, further growth in containment technology is seen to be vitally necessary to developing safe, high performance space flywheel systems.

PREVIOUS CONTAINMENT TECHNOLOGY DEVELOPMENTS

Most of the effort applied to developing containment design technology under the DOE/LLNL program was devoted to the radial burst problem [5]. This involves the response of the containment device (ring) to the radial impact of the bursting rotor and is aimed at defining the containment ring design. More recently, attention was given to the related problem of axial effects produced immediately subsequent to the radial burst actions [10]. These secondary effects can produce large loads on other parts of a containment housing, especially the end walls.

Radial Burst

Results of burst tests of composite rotors which had been performed at the Johns Hopkins U. Applied Physics Laboratory (APL) [8] were studied. The tests, listed in Table 1, involved a variety of rotor materials, constructions, and failure modes. The test results were especially useful because the rotors released a substantial and defined amount of fragmentation within containment rings that

were not excessively massive. Consequently, the rings were substantially deformed in the more severe bursts, while in the less severe ones, the rings, although not detectably deformed, nevertheless permitted deduction of an upper bound of containment severity. The tests provided a data base which helped in the development of the containment analysis.

When interacting with a containment ring, metallic fragments due to their material isotropy can exert contact pressures that exceed their yield stress. Also because of their high toughness, they typically remain intact during the entire process, thereby maintaining high bearing and shearing pressures. In contrast, composite fragments because of their relatively low transverse and interlaminar strengths cannot exert such high pressures. When pressures induced in the fragment exceed these strength limits, the matrix can be expected to break up, thereby releasing fibers or ribbons of fibers (filament-wound construction) or local delamination and crushing (laminated construction, edge loading). Rapid heating at the fragment/ring interface due to high pressure, high speed sliding also contributes to rapid fragment break-up. In some constructions, the initially released fragments may already be in a highly broken state prior to engagement.

Since the fragments are basically solid, as opposed to porous bodies, such action may be accompanied by the forcible ejection of material laterally from the fragment as the remaining fragment moves radially toward the containment structure. If the transverse strength is low, the fragment may continue this motion until its mass is expended. If the strength is high, however, the ejected mass may be appropriately less and a substantial portion of the original fragment remains after its radial velocity relative to the containment surface has vanished. Such residual fragments may continue to move tangentially after this time and exert centrifugal pressures against the containment ring.

An analysis, called the crushing fragment containment analysis (CFCA) was developed to calculate the containment ring response to such a loading process and is described in detail in [5]. Only a brief account is given here to provide a basis for describing the calculated results. The analysis (which neglects friction effects) assumes that at failure the rotor releases an axially symmetric distribution of fragments (See Fig. 2-I) which contacts the containment ring after moving through the radial clearance space, c that initially exists between the rotor and ring. At this instant (time, $t = t_o$) the centroid of the fragment system has radial and tangential velocities V_{Ro} and $V_{\theta o}$ respectively (Fig. 2-II). Subsequently, the fragment is further assumed to undergo a continuous radial crushing process, provided that the interface pressure that exists between the fragment and the ring exceeds a parameter p_o, called the apparent fragment crushing strength (Fig. 2-III). During the crushing process, the fragment system is assumed to eject material from its lateral (axial) faces, thereby losing mass and radial thickness, and its centroidal velocity, V_{Rt} may have increased or decreased from its initial value. Also the containment ring may have developed a velocity, $\dot{R}_t$. The interface pressure will be greater than p_o as long as $V_{Rt} > \dot{R}_t$ (Fig. 2-III). When the quantity $V_{Rt} - \dot{R}_t = 0$, the fragment system remains rigid ($t=t_p$). This begins the rigid phase (Fig. 2-IV), during which the fragment has only tangential velocity ($V_{\theta p}$) relative to the ring and exerts centrifugal pressure against it. If $V_{Rp} = 0$, then the burst containment process is ended at this time, since both fragment and ring will be radially at rest. If

however V_{Rp} ($=R_p$) >0 is at the beginning of the rigid phase, then the ring (with the fragment still rotating relative to it) will either come to rest ($t=t_f$, Fig 2-V) within the allowable radial growth (containment), come to rest beyond the allowable growth but within the ultimate tensile growth (unacceptable containment), or exceed the tensile growth limit (non containment).

The interaction geometry is illustrated in Fig. 3 which shows how the fragment proceeds to move into the ring. The initial state of the fragment is indicated by its bounding radii R_I and r_{iI}, thickness a_I, and centroid position, r_I. The initial total, radial and angular velocities are V_o, r_I, and ω_I respectively. These same quantities apply everywhere around the circumference since the fragment geometry and motion are considered to be axially symmetric. The various dashed lines indicate the trajectories of the fragment inner surface and mass center and the containment ring as time progresses. At a general instant, the fragment thickness is shown as having a centroidal radius, r, thickness, a, angular speed, ω, and total and radial speeds V and $\dot{r}$. It is noted that although V is always less than V_o, the radial speed may increase above the initial radial speed for a while. The final state of the fragment is depicted by the residual thickness, a_p, at the point where its radial velocity equilibrates with that of the containment ring.

The motion of the entire fragment is therefore characterized by that of the general mass center, m, whose variable mass per unit circumference $2\pi r$ is:

$$m = 2\rho_F h(R-r), \tag{1}$$

where ρ_F is the distributed fragment density. The equations of motion of the fragment and containment ring (neglecting friction) are:

$$\text{Fragment:}\quad \ddot{r} + \left(\frac{\dot{R}-\dot{r}}{m}\right)\dot{m} = \frac{H^2}{r^3} - \frac{p_o h}{m} \tag{2}$$

$$\text{Ring:}\quad \ddot{R} = \frac{2\pi}{M_C}\left[(\dot{R}-\dot{r})\dot{m}r + p_o hr - \sigma T L_e\right] \tag{3}$$

where the single and double dots indicate first and second time derivatives respectively; $H = \omega r^2$ = constant; p_o, fragment crushing strength; h, rotor axial length; σ, dynamic tensile strength of ring; T, ring thickness; and M_C and L_e, the effective mass and length of the ring. Hence, the fragment is treated as a variable mass which transfers momentum loads, $(\dot{R}-\dot{r})\dot{m}$ and pressure loads, $p_o h$ (both per unit circumference) to the containment ring. The ring resists these loads by its plastic tensile resistance $\sigma T L_e$.

The initial conditions are:

$$\text{Fragment: } r(o) = r_I,\ \dot{r}(o) = V_{RI}$$

$$\text{Ring: } R(o) = R_I,\ \dot{R}(o) = o \tag{4}$$

During the ensuing process, the condition $\dot{r}_p = \dot{R}_p = V_{Rp}$ is reached, at which time and thereafter, the fragment is considered to be rigid. Subsequently, the fragment continues moving circumferentially at angular velocity ω_p and exerting centrifugal pressure loading on the ring:

$$p_p = \frac{m_p (\omega_p r_p)^2}{r_p h} \tag{5}$$

During this time the radial motion of fragment and ring is governed by:

$$\ddot{R} = \frac{2\pi}{(M_c + M_p)} \left[p_p h r_p - \sigma T L_e \right] \tag{6}$$

where $M_p = 2 \pi r_p m_p$.

For present purposes, equation (6) was solved assuming the bracket term to be constant. Although not necessary to do this, it is conservative and it was convenient to do so. Hence the final time at which the radial velocity ceases is:

$$t_f = t_p + \frac{M_c + M_p}{2\pi} \left[\frac{V_{R_p}}{\sigma T L_e - p_p h r_p} \right] \tag{7}$$

and the maximum radial deflection of the ring:

$$\Delta R_{max} = R_p - R_I + 1/2\ V_{Rp} (t_f - t_p) \tag{8}$$

The ring deflection, ΔR, applies to the effective length, L_e, which depends on the ring overhang/thickness ratio, $a/T = (L-h)/2T$. As described in [5], $L_e = L$ for $a/T \leq 3$ (narrow rings) and $L_e = h+6t$ for $a/T > 3$ (wide rings). These distinctions are based on [11]. Physical evidence shows that the axial deflection profile has a peak at the center of the ring, when the rotor is centrally situated. The peak deflection $\Delta R'$ is estimated as follows [5]:

$$\text{Narrow Rings:} \quad \frac{\Delta R'}{\Delta R} = \frac{h + 2a}{h + 2a(1-a/6T)} \quad ; \quad \text{Wide Rings:} \quad \frac{\Delta R'}{\Delta R} = \frac{h+6T}{h+3T} \tag{9}$$

CFCA has yielded some very interesting features of containment processes of composite rotors, features which appear plausible, especially when compared with experimental evidence of fragmentation as obtained for rotors of various constructions. The following results illustrate some of these features.

Figures 4 and 5 show plots of r, $\dot{r}$, R, and $\ddot{R}$ vs. time for the complete burst of a 0.25 kw.hr laminated glass/epoxy disk rotor, the principal differences being the fragment strength and ring thickness values: p_o = 0 and T = 0.22 in. (Fig. 4)

and p_o = 12 ksi and T = 0.35 in. (Figure 5). In each case, $\dot{r}_I$ = 3847 in/sec. initially (which corresponds to an initial radial clearance, c = 0.25 in.) and subsequently rises to a peak value. The peak value of r is larger for p_o = 0 and occurs at a later time than for p_o = 12 ksi. Also, r approaches closer to R for p_o = 0 such that at the equilibration condition, $\dot{r} = \dot{R} = V_{Rp}$, the residual fragment thickness, a = 2 (R - r) is much smaller than that of the stronger fragment. This is typical of fragment behavior as revealed by CFCA. It is noted that even though p_o = 0, substantial deformation is produced in the ring. This, of course, is attributable to the fragment momentum loading.

Another interesting result is to show that fragments having low strength can transmit substantial deformation to the ring even when the initial radial clearance is zero. An example is illustrated in Figure 6, which pertains to the same conditions as the previous figures except p_o = 6 ksi, T = 0.24 in., and c = 0. Here $\dot{r}$ is initially zero (because of the zero clearance) but rises to a peak value of 4,870 in/sec. $\dot{R}$ remains at zero for the first 400 μ sec. and rises thereafter to a peak value of 1,570 in/sec., almost as high as for the case shown in Figure 4. The maximum ring deflection, ΔR = 0.62 in., compared to 0.60 in. (Figure 4). Since for these two cases, the ring thicknesses, T, are almost identical, it is seen that the effect of the higher fragment strength tends to be offset by the smaller clearance value.

The CFCA was used to analyze the radial burst containment behavior of a variety of composite flywheels that had been spin tested [8]. The tests were performed within the confines of a steel ring which was used primarily to protect the test chamber from damage. To satisfy this need and also permit access to and visual coverage of the test chamber interior during the test, the radial and axial spaces between the flywheel and chamber walls were much larger than is representative of a practical containment housing design. Such tests provided the only available experimental base for studying composite rotor containment effects, however, and were so utilized despite the fact of their affording only a rough simulation of a realistic environment. Within these limitations, the CFCA when applied to the tests permitted an evaluation of the apparent fragment crushing strength, p_o for such rotor components as laminated glass/epoxy and graphite/epoxy disks, chopped-glass fiber/SMC molded disks and filament-wound graphite/epoxy and aramid/epoxy rings. The resulting values of p_o which are dependent on the orientation of the composite component relative to the radial direction as well as the radial impact speed are listed in Table 2 along with other test data such as radial clearance C, and radial fragment speed at initial contact, V_{RI}. It is to be expected that the resulting values of p_o are affected by the testing environment as noted above and that they might be significantly different if evaluated in a more representative containment space. For example, two effects of excessive radial clearance would exert opposing influences on the value of p_o, namely, (1) it would facilitate the axial ejection of debris from the fragment crushing site and yield a lower value of p_o and (2) it would result in a larger radial fragment impact velocity and hence a higher value of p_o.

The two tests listed in Table 2, which involved aramid fiber/epoxy rings, viz. the Brobeck and Garrett flywheels, provide an example of how the evaluation of p_o is affected by test conditions. In the Brobeck rotor test, the clearance, C

was 31 percent of the outside rotor radius whereas in the Garrett rotor test the corresponding value was only six percent. Also, the ratio of C to the rotor axial length for the two cases was 43 and 36 percent respectively. Assuming the material effects to be similar in the aramid/epoxy rings of these rotors, the above values would favor a lower evaluation of p_o for the Brobeck test on the basis of (1) above. On the other hand, the higher radial fragment speed in the Brobeck compared to the Garrett rotor tests (see Table 2) would contribute to a higher value of p_o for the former case. The Brobeck test correlation yielded a zero value of p_o and even further indicated that the rotor rim engaged the containment ring in discrete stages rather than all at once. For the Garrett test p_o was found to be 12,000 psi, indicating that the rim fragments engaged the ring in a much more contiguous state and required very high interface pressures to break them down.

An example of how the CFCA test correlation is done is given for the Garrett test. Calculations of peak containment ring growth were made for several assumed values of p_o which ranged from 0 to 21,000 psi. Results are shown in Figure 7 in which $\Delta R'$ (equation 9) is plotted against p_o. $\Delta R'$ (= .75 in.) of the actual ring was determined [12] by measuring the circumference near the ring axial center where the maximum deflection was present. A value of p_o equal to 12,000 psi was then picked off from Figure 7 for the measured value of $\Delta R'$.

An example of how the CFCA has been applied to design estimation is shown in Figure 8 which presents estimates of containment ring weight, W_C relative to the complete burst of a laminated glass/epoxy disk rotor at a stored energy of .25 kwh and whose OD and weight are 18 in. and 28.9 lb., respectively. The estimates are based on p_o = 6 ksi (rather than p_o = 0 as listed in Table 2), a conservative value to account for possible effects of fragment compaction in the small radial clearance assumed (three percent of rotor outside radius). W_C is plotted against the maximum radial ring growth for several ring materials. An advanced design incorporating an inner metallic liner over wound aramid fiber yarn is also shown. The dots on the curves indicate the maximum allowable ring growth which corresponds to an average tensile strain of 10 percent for the metallic rings and four percent for the aramid fiber/6061 aluminum ring. The burst performance of the latter ring construction is indicated to be 34 wh/lb (burst energy divided by ring weight). In contrast to this the performance of a low carbon steel ring (dynamic tensile strength of 85 ksi) is about 10 wh/lb.

Axial Effects

Although previous spin tests had shown evidence of important axial loading effects resulting from composite rotor bursts, not until the containment test of a General Electric hybrid flywheel were such effects amenable to detailed study. This particular test involved a high energy burst at a stored energy level of 648 wh within an experimental vehicular type housing and it remains the only such test ever performed. The housing failed to contain the burst due apparently to large axial loading effects that were further aggravated by asymmetric burst conditions. The containment ring which was a separate component within the housing assembly was, on the other hand, relatively unaffected by the burst except for small permanent out-of-roundness and radial expansion deformations.

A method for estimating the axial loads transferred to the housing end walls was devised using the crushing fragment analysis. In the CFCA the fragment system mass loss is accommodated by the axial ejection of crushed material, as previously noted. An upper bound estimate of the axial loading due to the flow of ejecta was made by assuming that the radial momentum of the entire crushed mass is conserved in the corresponding axial flow. The momentum of the crushed mass is obtained from the CFCA by summing up the products, $\bar{r}\Delta m$ of the mass lost, Δm, in a given time interval and the average radial speed, $\bar{r}$ of the contiguous fragment system at the beginning and end of the time interval. Actually, only a portion of the mass-loss momentum would be transferred to the end walls because some momentum would be dissipated in turning the velocity vector from the radial to the axial direction. The mass-loss momenta contributed by the rotor ring and disk components are plotted against time in Figure 9. The time base only signifies duration and does not chronologically relate the ring and disk portions. The contribution of the ring is quite small compared to that of the disk. This reflects the fact that the crushed mass of the ring is only 27 percent of the disk crushed mass. The disk contribution is shown for assumed values of p_o = 0 and 6 ksi. It is noted that the mass loss momentum corresponding to p_o = 6 ksi is the larger of the two. This is because the crushed mass is less for larger values of p_o, a fact due to the existence of the residual fragment (see Figure 2-V). This relationship holds even when the ultimate breakdown of the residual fragment is considered. For very large values of p_o, which characterize a rigid fragment system, the mass-loss momentum becomes negligible and hence the axial momentum associated with it as well. This behavior models that of rigid burst fragments which produce large radial loading effects but very small axial effects (assuming the motion remains in the plane of rotation).

The axial momentum as derived above from the mass-loss momentum can be applied to the end wall structures as an impulse load. This is justifiable because the duration of the crushing process is likely to be small compared to the period of the fundamental flexure vibration mode of the end wall. This was done in studying the behavior of the experimental housing during the General Electric hybrid rotor containment test. It was found the axial load due to the rotor ring mass-loss momentum was large enough to produce relatively minor plastic deflection of the end wall but insufficient to cause the observed level of damage. The load due to the disk mass-loss momentum, however, was found to be greater than necessary to produce damage.

It is noted that the above assessment of axial load effects represents but an initial attempt based on very limited test experience. It is viewed as being an overestimate of the load magnitude that can result from the primary breakdown of a composite rotor during the containment process. Other mechanisms are possible such as fragment debris compaction, which might produce large, localized loads and damage.

CONCLUSIONS AND RECOMMENDATIONS

1. The preferred approach to developing high performance space flywheels is to utilize 'fail-safe' or 'limited-failure' rotor designs in order to minimize containment requirements. The penalty of having to contain a complete rotor burst, on the other hand, is very likely to be prohibitive.

2. 'Fail-safe' or 'limited failure' rotor concepts are available and their development should be pursued as a first step toward development of the flywheel power system. To establish assured designs will require a considerable extension of the mechanical properties data base of candidate rotor materials. Cyclic spin testing (adequately instrumented) of rotors or major rotor components should be emphasized.

3. Until assured 'fail-safe' rotor performance is demonstrated, containment is likely to be a design requirement for a manned environment. Meanwhile, containment requirements should be defined, where possible, on the basis of the failure modes of 'limited-failure' type rotor designs and appropriate shields designed.

4. Containment design technology is presently inadequate for defining an optimum housing design. The crushing fragment containment analysis (CFCA) can be applied to making preliminary designs which then should be subjected to rotor burst test conditions as a means of developing efficient hardware.

5. Containment technology development should be continued further, especially by means of coordinated experimental/analytical investigations of composite rotor containment test behavior. In support of this, rotor spin testing should be performed within a containment housing whenever possible.

ACKNOWLEDGEMENT

This work was sponsored by the U.S. Department of Energy through the Lawrence Livermore Laboratory. The author gratefully acknowledges Drs. Satish V. Kulkarni and Carl Walter of the Lawrence Livermore Laboratory and Mr. J. F. Martin of the Oak Ridge National Laboratory (ORNL) for their generous support and Messrs. W. O. Wilkinson of Johns Hopkins University Applied Physics Laboratory, E. F. Babelay of ORNL, E.L. Gray of General Electric Space Systems Division, and to Dr. R. S. Steele, formerly of ORNL, for their technical contributions.

REFERENCES

1. "Proceedings, 1977 Flywheel Technology Symposium", U.S. Department of Energy, CONF-771053, March 1978.
2. "Proceedings, 1980 Flywheel Technology Symposium" U.S. Department of Energy, CONF-801022 (1980).
3. "Proceedings, Mechanical, Magnetic and Underground Energy Storage 1980 Annual Contractors' Review," U.S. Department of Energy, CONF-801128, November 1980.
4. "Proceedings, Mechanical, Magnetic and Underground Energy Storage 1981 Annual Contractors' Review," U. S. Department of Energy, CONF-810833, February 1982.
5. Coppa, A. P., "Energy Storage Flywheel Housing Design Concept Development", Lawrence Livermore National Laboratory, UCRL-15448, March 1982.
6. Sapowith, A.D., and Handy, W.E., "A Composite Flywheel Burst Containment Study", Lawrence Livermore National Laboratory, UCRL 15452, April 1982.
7. Davis, D., and Hodson, D., "Rocketdyne's High-Energy Storage Flywheel Module for U.S. Army", 1977 Flywheel Technology Symposium Proceedings, CONF-771053, UC-94b, 96, March, 1978.
8. Rabenhorst, D.W.; Wilkinson, W.O., "Prototype Flywheel Spin Testing Program", Johns Hopkins University, Applied Physics Laboratory Report No. SDO 5988, also UCRL-15381 (Lawrence Livermore National Laboratory, April 1981.
9. Coppa, A.P., "General Electric Composite Ring-Disk Flywheel: Recent and Potential Developments". Proceedings of the NASA Flywheel Inertial Energy Storage Workshop, February 7-9, 1984.
10. Coppa, A.P., "Flywheel Containment Design and Technology Developments", Proceedings of the DOE Physical and Chemical Energy Storage Annual Contractors' Review Meeting, CONF-830974, September 1983.
11. Hagg, A.C. and Sankey, G.O., "The Containment of Disk Burst Fragments by Cylindrical Shells", ASME Journal of Power, April 1974.
12. Wilkinson, W.O., "Final Report, Flywheel Burst Test Program, APL Spin Test Facility", Johns Hopkins University, Applied Physics Laboratory, Report No. JHU/APL AEO-83-57, June 1983.

Table 1. Flywheel Rotors Involved in the Data Correlation (8)

Rotor Description	d_o in.	W_R lb.	KE_B kwh	ω_B rpm	Failure Mode	W_F lb.
Hybrid Rotor: FW Graphite/Epoxy Ring; Laminated S-2 Glass/Epoxy Disk (General Electric)	17.68	23.3	0.459	35,040	Outer Ring Rupture	6.34
Disk Rotor: Laminated S-2 Glass/Epoxy Disk (LLNL)	15.00	5.2	0.156	49,320	Complete Disk Burst	5.2
Hybrid Rotor: FW Graphite/Epoxy Outer Ring; Molded Chopped Glass/SMC Disk (Owens Corning)	24.00	28.5	0.414	21,620	Complete Burst of Rim and Disk	28.5
Wound-Rim Rotor: FW Kevlar 49/Epoxy, Glass/Epoxy (Brobeck)	13.76	24.5	0.608	48,120	Rupture and release of 70% of Kevlar49/Epoxy Rim	6.76
Disk Rotor: Varying Thickness, Laminated Graphite/Epoxy	24.00	11.8	0.306	34,940	Complete Disk Burst	11.8

d_o, OD, W_R, rotor weight; KE_B, energy at burst, ω_B, burst speed, W_F, total fragment weight.

Table 2. Values of p_o, Fragment Crushing Strength as Obtained from Data Correlation of APL Rotor Burst Tests

Material	Form	Impact Direction	P_o (psi)	C (in.)	V_R (in/sec)
Graphite/ Epoxy	Filament Wound Ring	Transverse	20,000	4.62	22,900
	Laminate	Longitudinal	45,000	1.50	15,790
S-2 Glass/ Epoxy	Laminate	Longitudinal	0	1.50	16,470
Kevlar® 49/ Epoxy	Filament Wound Ring	Transverse	0 12,000	2.12 0.75	21,540 12,000
Chopped Glass/ SMC	Molding	Longitudinal	5,000	1.50	9,880

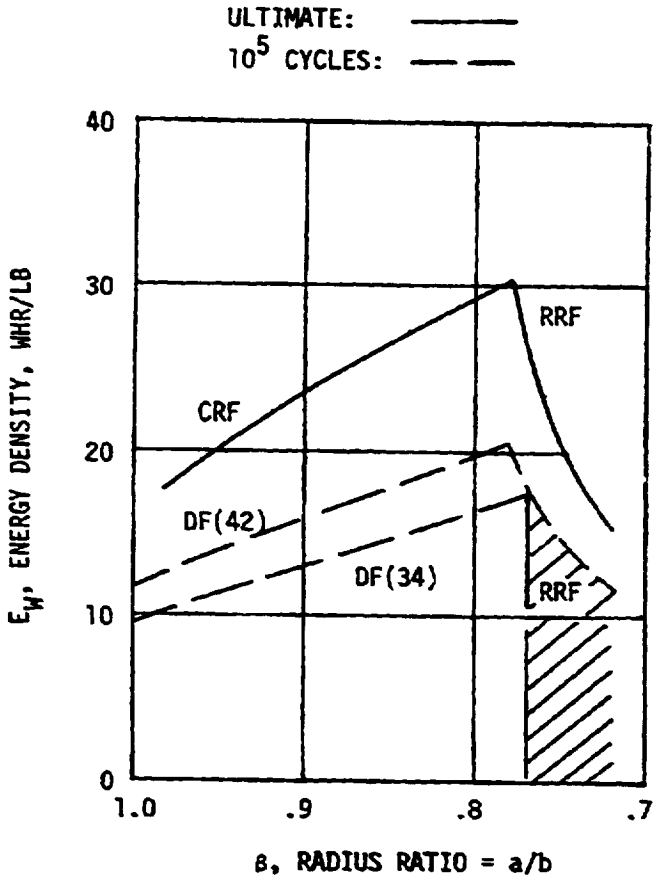

Figure 1. Hybrid Flywheel Energy Density vs. Radius Ratio

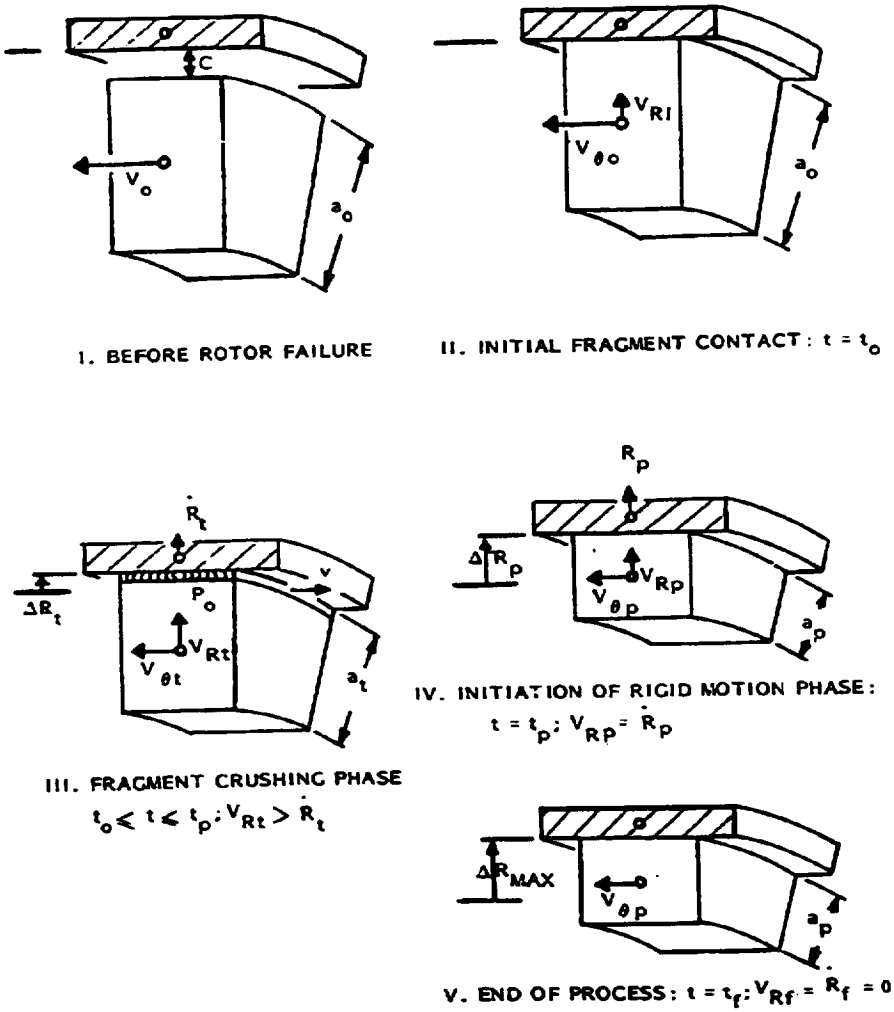

Figure 2. Diagram of Fragment Crushing Process Showing Five Phases

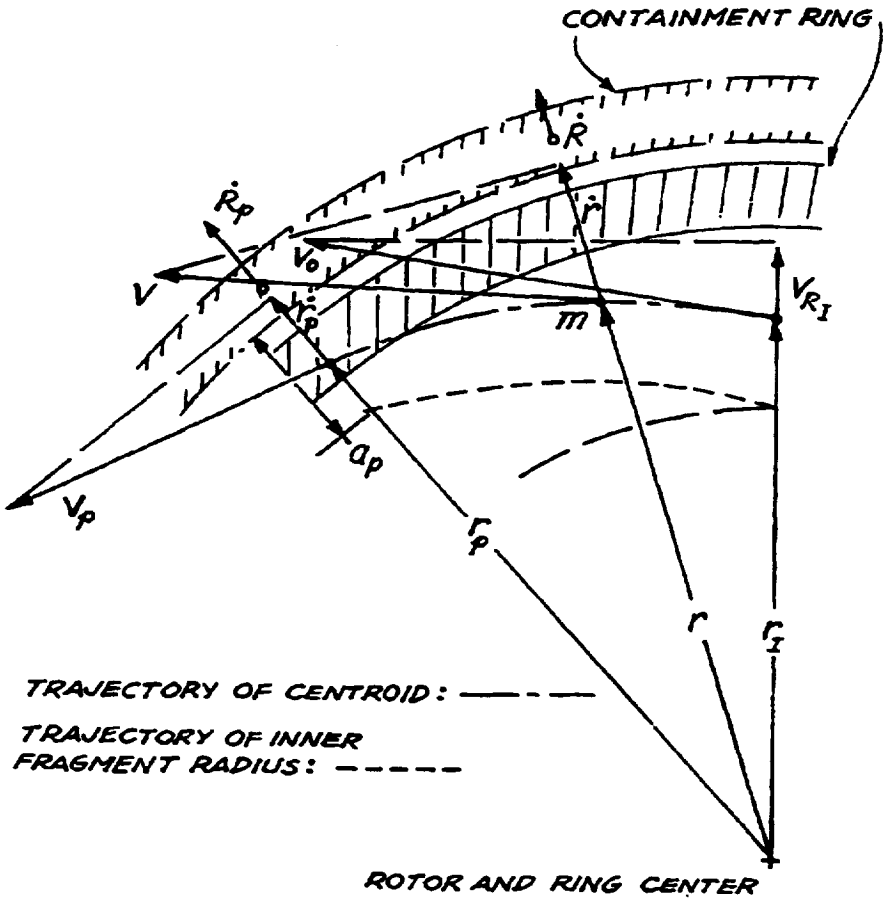

Figure 3. Crushing Fragment Interaction Schematic

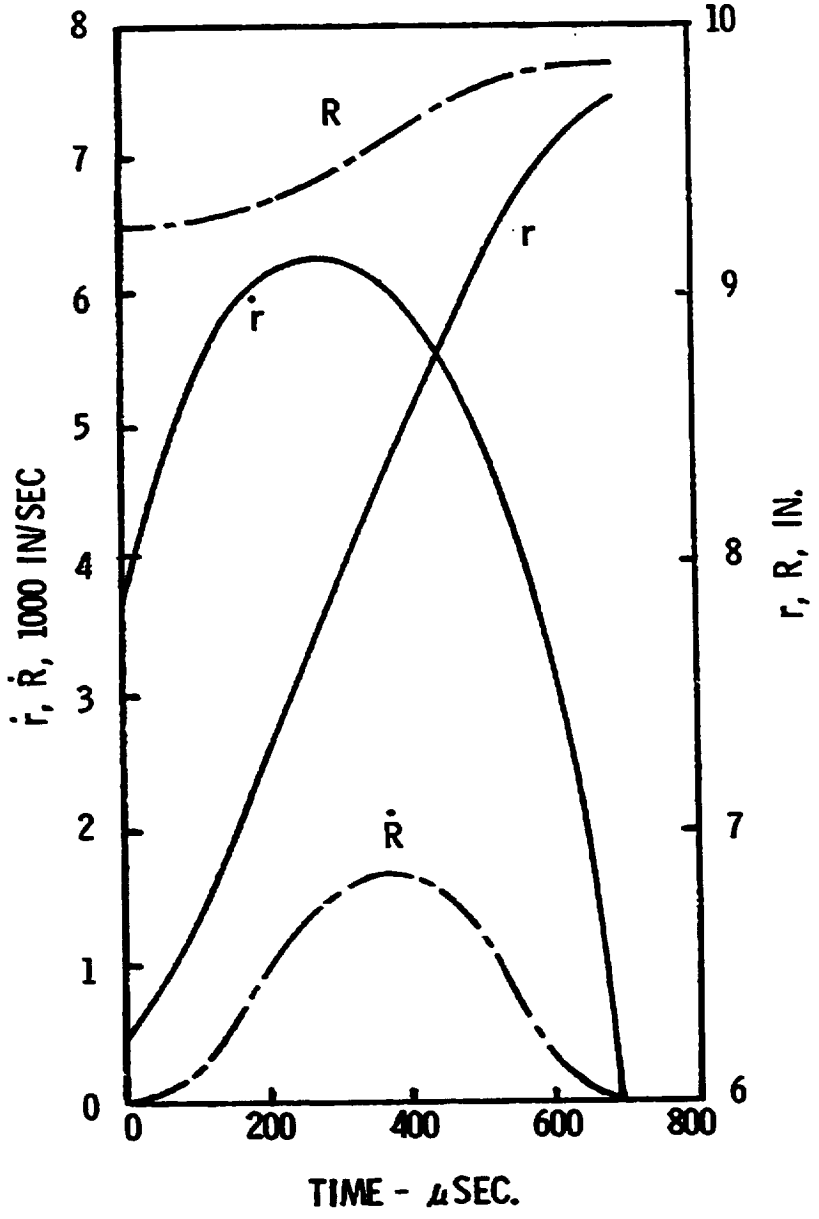

Figure 4. Calculated Fragment and Containment Ring Motions vs. Time for Complete Burst of a 0.25 kwh Laminated Glass/Epoxy Disk Rotor. P_o = 0; 4130 Steel Ring (σ = 158 ksi)

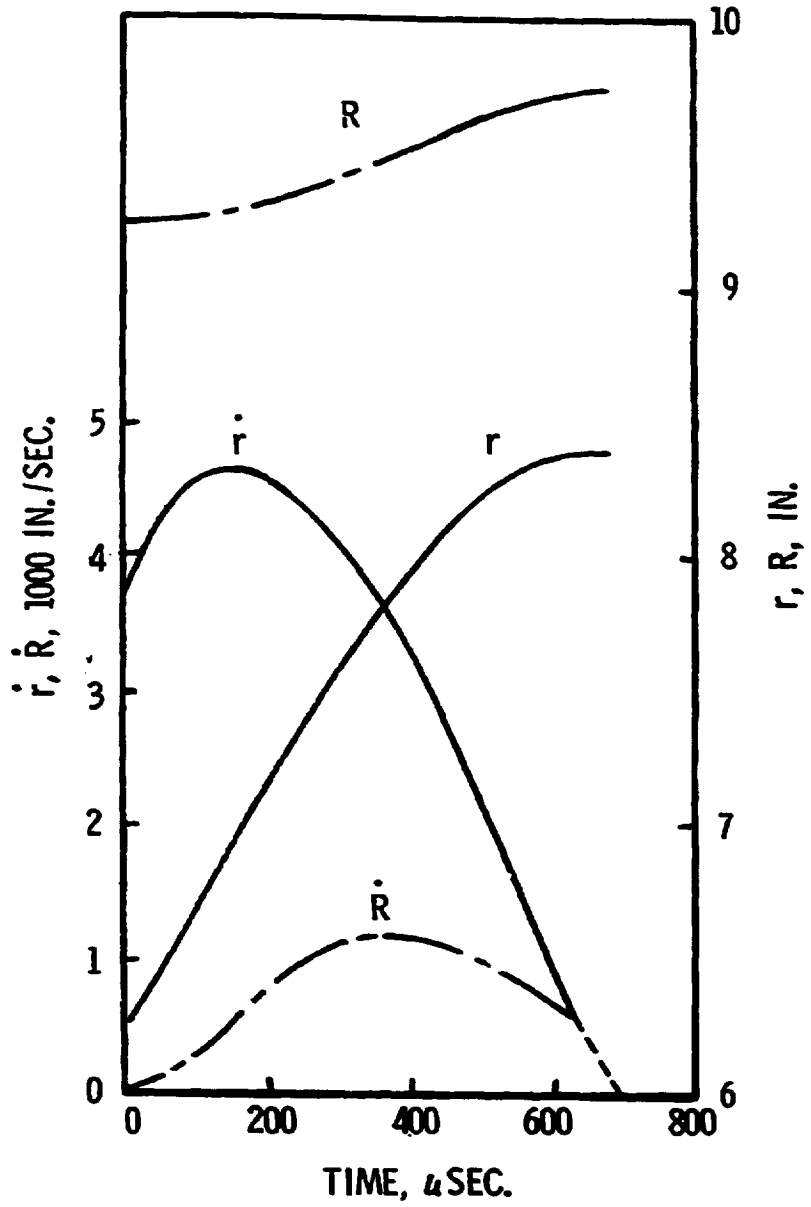

Figure 5. Calculated Fragment and Containment Ring Motions vs. Time for Complete Burst of a 0.25 kwh Laminated S-Glass/Epoxy Disk Rotor. p = 12,000 psi, 4130 Steel Ring (σ = 159 ksi)

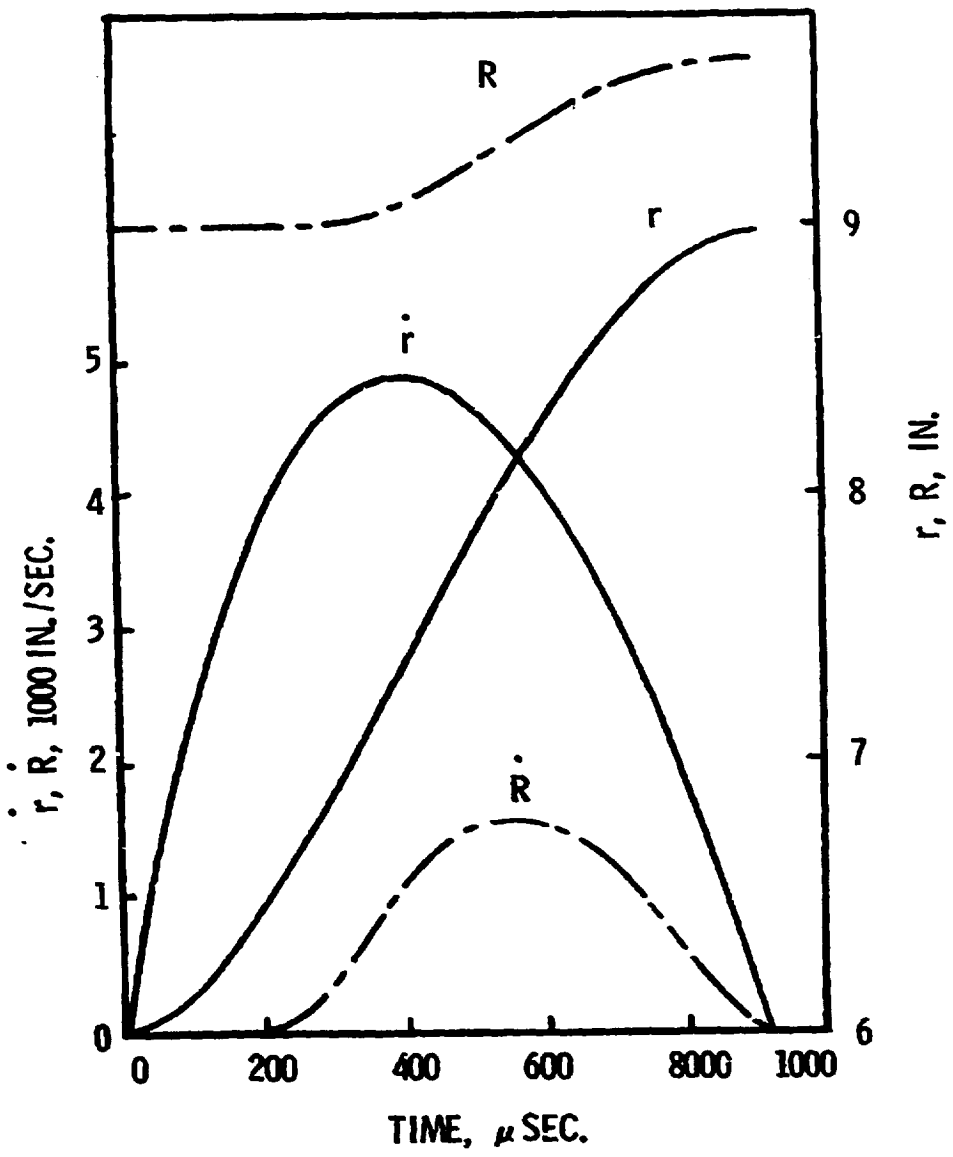

Figure 6. Calculated Fragment and Containment Ring Motions vs. Time for Complete Burst of a 0.25 kwh Laminated S-Glass/Epoxy Disk Rotor, p_o = 6,000 psi. Radial Clearance, C = 0, 4130 Steel Ring (σ = 158 ksi)

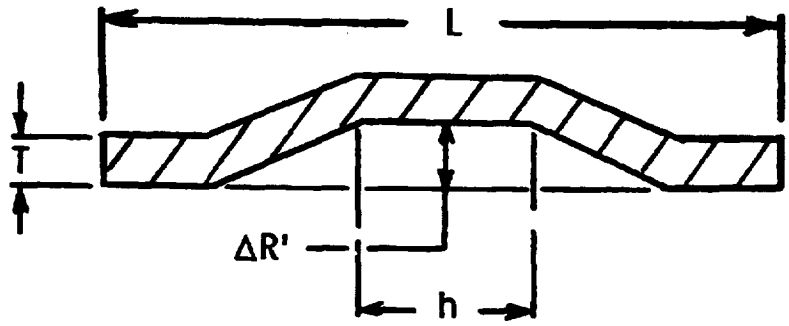

DEFLECTED RING SECTION

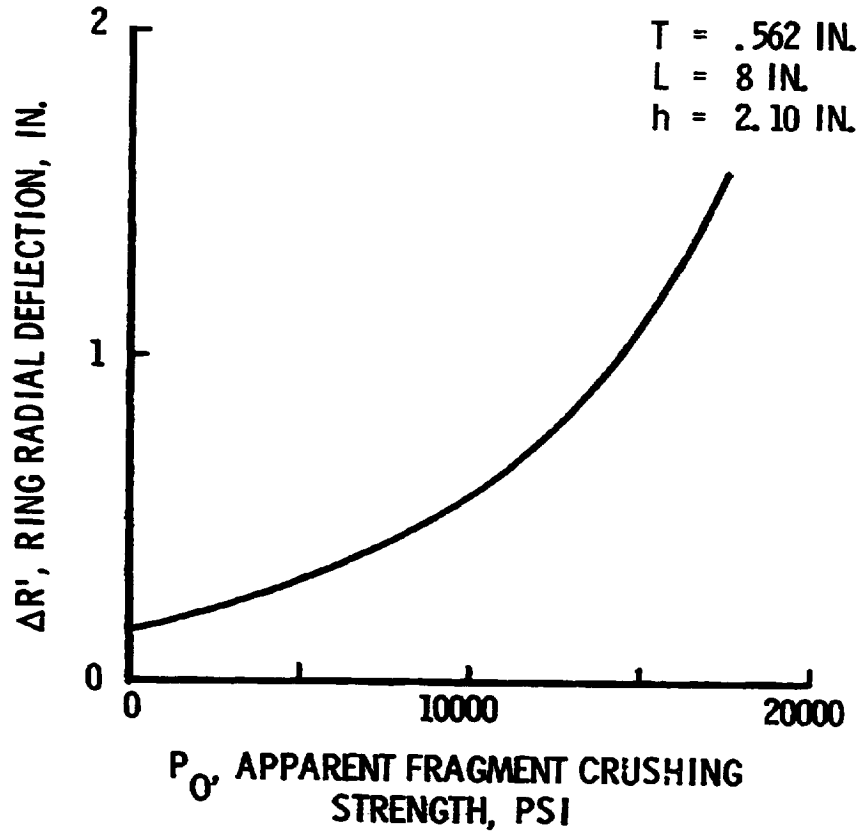

Figure 7. Calculated Peak Radial Deflection, ΔR' vs. Crushing Strength, p_o for Aramid/Epoxy Filament Wound Rim (Garrett Flywheel)

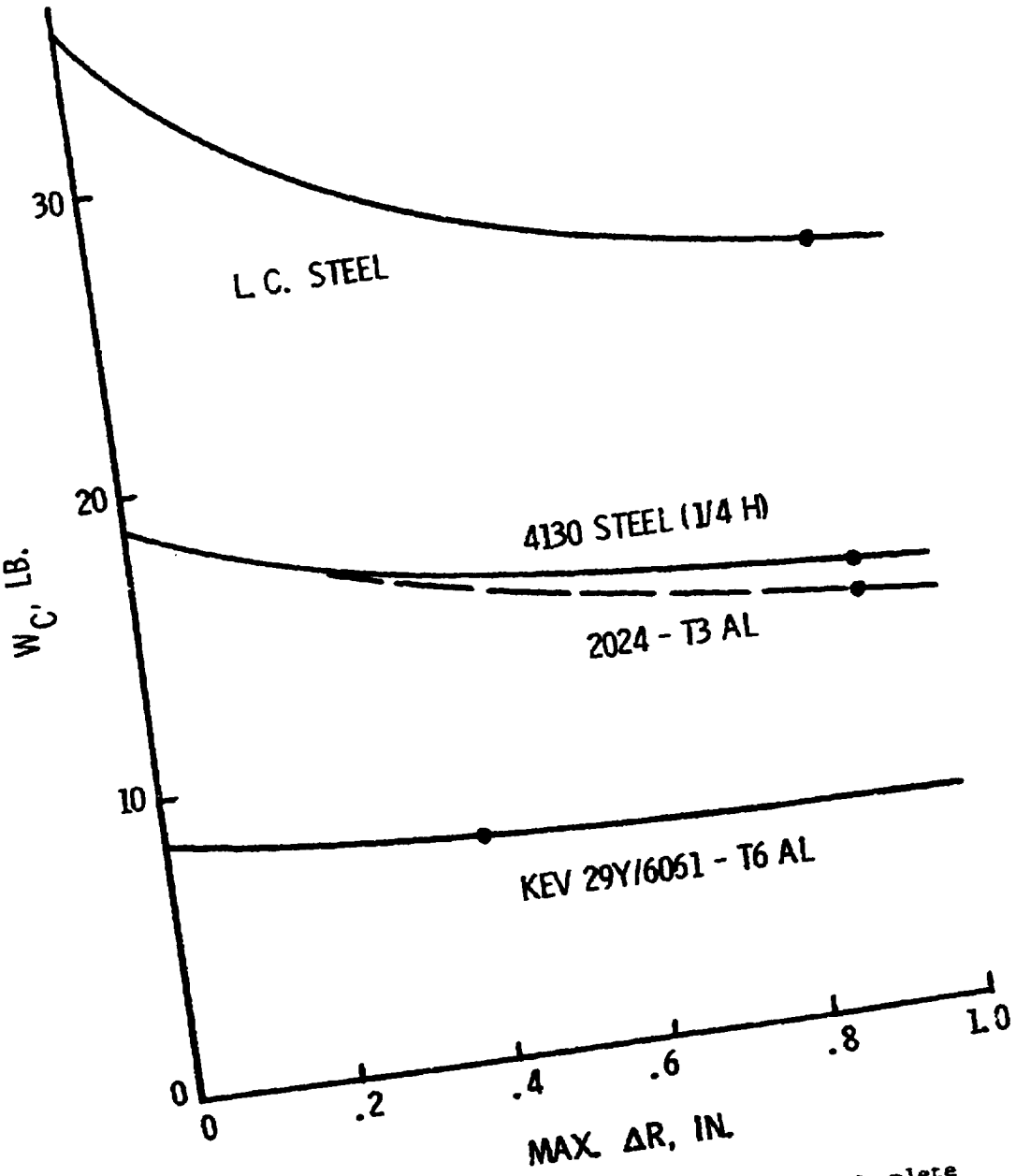

Figure 8. Containment Design Curves: W_c vs. ΔR_{max} for Complete Burst of an 18 in. OD, 0.25 kwh Laminated S-Glass/Epoxy Disk Rotor for Several Containment Ring Materials

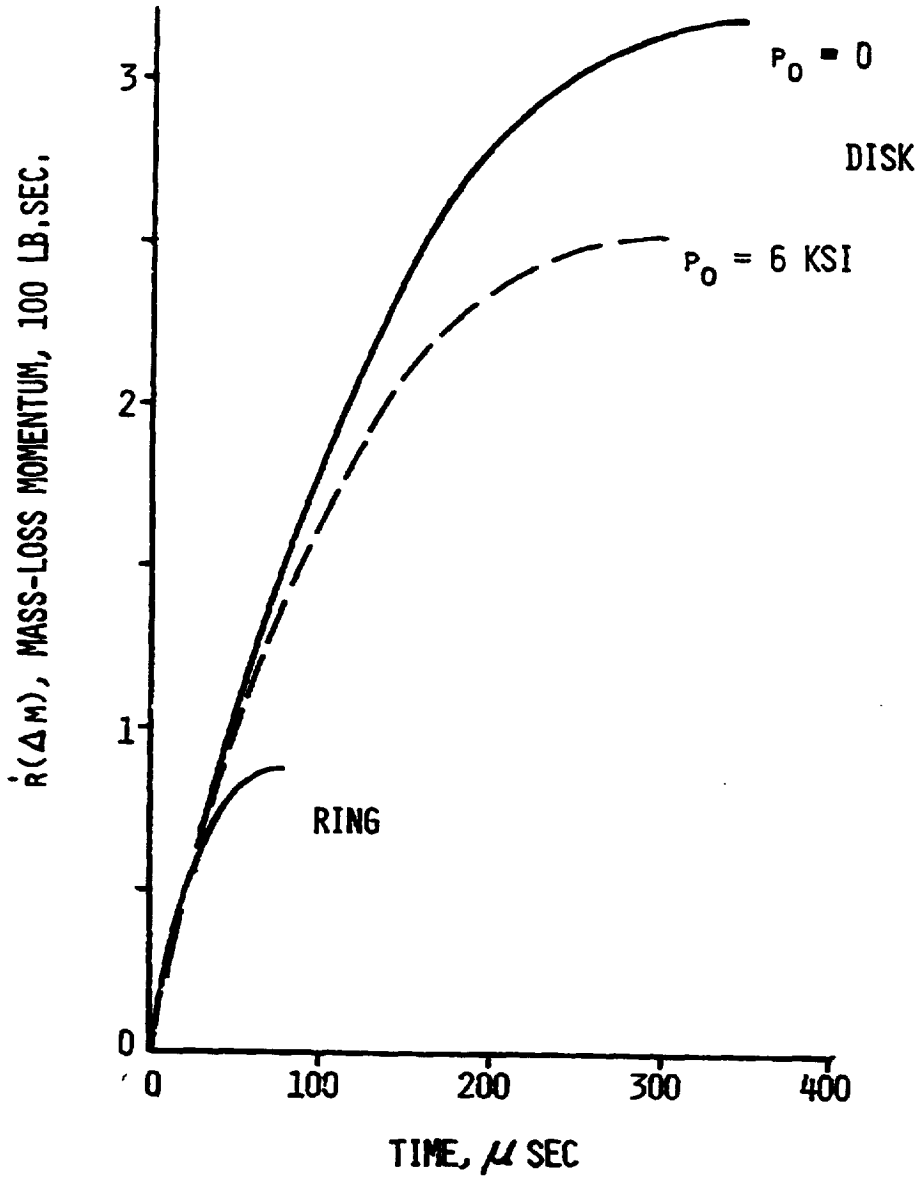

Figure 9. Calculated Mass-Loss Momentum During Containment of a GE Hybrid Flywheel at 648 wh Stored Energy